Trans. Japan Soc. Aero. Space Sci.
Vol. 45, No. 147, pp. 35–44, 2002

Correlation between Linear Stability Theory and Transition of Compressible Jet Shear Layer

By Mohammed K. IBRAHIM and Yoshiaki NAKAMURA

Department of Aerospace Engineering, Nagoya University, Nagoya, Japan

(Received June 21st, 2001)

A correlation between spatial linear stability calculations and the onset of transition in compressible jet shear layer was investigated. In the present study, an attempt was made to apply the conventional e^N method to a transition prediction of the free shear layer flow in a compressible jet. The mean velocity profiles for a compressible circular jet were experimentally obtained at different downstream locations, which were used as an input to the linear stability calculation code. The growth rates of disturbances from the stability calculation were integrated to obtain an envelope curve. On the other hand, the transition was detected experimentally by the use of three techniques: (1) oil flow visualization, (2) microphone measurements for pressure fluctuations, (3) hot wire anemometer measurements for velocity fluctuations. The results from both the microphone and the hot wire anemometer measurements showed that the transition starts at about $1.333D$ from the nozzle exit, where D is the nozzle diameter, which is near the "apparent origin" in the fully developed jet flow. It was found that the value of factor N in the e^N method is about 3.5 for axisymmetric ($n = 0$) and 2.8 for asymmetric ($n = 1$) disturbance modes in the present compressible jet.

Key Words: Compressible Jet, Shear Layer Transition, Linear Stability Analysis

Nomenclature

A : root mean square value of disturbance amplitude
C_1, C_2 : complex constants
C_g : group velocity
D : nozzle exit diameter
i : $\sqrt{-1}$
I_n : modified Bessel's function of first kind of order n
K_n : modified Bessel's function of second kind of order n
M_j : fully expanded jet Mach number; Mach number the jet will have when isentropically expanded to the ambient pressure
M : jet Mach number
n : azimuthal wave number of disturbance; jet instability mode
N : factor of e^N method
p : pressure
Pr : Prandtl number
P_t : jet total pressure; chamber pressure
Re : Reynolds number
R : jet radius, which is defined as the length from the axis to where the velocity becomes half the centerline velocity, i.e., $U(R) = U_0/2$
T : temperature
t : time
U : velocity
v : fluctuating quantity such as velocity, pressure, density, and temperature
x, r, ϕ : axial, radial, and azimuthal coordinates
α : $\alpha_r + i\,\alpha_i$
α_r : axial wave number of disturbance
α_i : axial spatial growth rate of disturbance
γ : specific heat ratio
ρ : density
ω : radian frequency of disturbance
θ : momentum thickness

Subscripts
o : jet centerline
∞ : ambient or in the far field
0 : initial value
i : imaginary part
r : real part
k : station number in the radial direction
j : station number in the axial direction

Superscripts
$-$: time mean
$'$: fluctuating component
$\sim$: amplitude of fluctuating component

1. Introduction

The problem of transition from a laminar to a turbulent flow is of great practical interest and has a wide range of engineering applications. The first stage of a transition process is the boundary layer receptivity. This receptivity is a mechanism that enables environmental disturbances to enter a laminar boundary layer, or laminar shear layer, and to generate unstable waves.[1)] When the amplitude of these disturbances is small, the linear amplification or growth of those unstable waves constitutes the second stage of the transition pro-

cess, which can be explained by the *linear stability theory*. The third stage occurs when the unstable waves reach a finite amplitude; their behaviors begin to deviate from the prediction by the linear theory, where wave/wave interactions and nonlinear evolution occur, leading to a turbulent flow.[2)]

If we assume that the linear stability theory can be valid up to the onset of transition, its major shortcoming is that it cannot predict the location of transition. What the linear stability theory can do, however, is to compute the amplitude *ratio*, i.e., the amplification rate between two locations, *only*, where the absolute values of these amplitudes remain to be unknown. If it is assumed that the transition occurs when the amplitude of the most unstable disturbances reaches a prescribed threshold, it is easily understood that the linear theory alone is unable to predict the transition location. However, in spite of this negative situation, transition predictions have to be made. This can be achieved by adding a somewhat *empirical* ingredient to the linear theory, which is the basis for the e^N method.

The e^N method was first developed independently by Smith and Gamberoni[3)] and by Van Ingen[4)] in 1956 to predict the transition location for wall-bounded shear flows. Today the e^N method is still a state-of-the-art transition prediction design tool for wall-bounded shear flows encountered in industrial applications. As far as we know, however, no attempt has been made to develop an analogy of the e^N transition-prediction method for free shear flows such as jet and wake. This is a main objective of the present study, where we focus on circular jets as free shear flows.

Jets and mixing layers are characterized by their mean-velocity profiles with an inflection point that causes inviscid instabilities. The primary mechanism of these instabilities is vortical induction, where viscosity plays only a role of damping. Thus jet flows at high Reynolds numbers can be well described by the inviscid flow equations, i.e., the Euler equations. Therefore the linearized form of these equations considered in the linear stability analysis will be meaningful.

2. Linear Stability Theory

The principle of the linear stability theory is to introduce small sinusoidal disturbances into the linearized inviscid Euler equations to compute unstable frequencies. Here it is assumed that any fluctuating quantity v' such as velocity, pressure, density, and temperature is expressed by

$$v' = \tilde{v}(r)e^{in\phi+i(\alpha x-\omega t)} \tag{1}$$

The complex amplitude function $\tilde{v}$ depends on r only, and n is an integer that represents an azimuthal wave number. Basically, α and ω are complex values.

Since the fluctuation quantities are very small, the quadratic terms regarding these quantities will be neglected in the inviscid equations. It is also assumed here that the mean flow quantities do not change significantly over a wavelength of disturbances; therefore $\bar{U}$, which is the mean velocity component in the x direction, as well as temperature $\bar{T}$ and density $\bar{\rho}$, are functions of r. The mean pressure $\bar{p}$ is assumed to be constant in this study, which corresponds to the case for a fully expanded jet.

This parallel basic flow approximation implies that the stability at a particular location of x is determined by local conditions; that is, it is not affected by quantities in other regions. This leads to a system of ordinary differential equations for amplitude function $v(r)$, where there are four equations for incompressible flows, i.e., the continuity equation and the r, ϕ, x momentum equations, and two equations of energy and state are needed for compressible flow in addition to them. These stability equations can be combined to obtain a single equation for the pressure fluctuation, p'.[5)]

$$\frac{d^2\tilde{p}}{dr^2}+\left[\frac{1}{r}-\frac{1}{W}\frac{dW}{dr}\right]\frac{d\tilde{p}}{dr}-\left[\alpha^2(1-{M_0}^2W)+\frac{n^2}{r^2}\right]\tilde{p}=0 \tag{2}$$

where

$$W(r)=\left[\frac{\bar{U}(r)-\dfrac{\omega}{\alpha}}{U_0}\right]^2\Bigg/\left[\frac{\bar{T}(r)}{T_0}\right] \tag{3}$$

When r tends to 0 (jet axis) or ∞ (ambient fluid), the quantity W of Eq. (3) approaches a constant value, where the asymptotic solutions to Eq. (2) are given by the modified Bessel functions, I_n and K_n, of order n. Since it is required from the boundary conditions for the pressure disturbance equation that $\tilde{p}(0)$ is bounded and that $\tilde{p}(\infty)$ goes to zero, we have, for $r \to 0$

$$\tilde{p}(r)=C_1 I_n\left(\sqrt{1-{M_0}^2W(0)}\,r\right) \tag{4}$$

and for $r \to \infty$

$$\tilde{p}(r)=C_2 K_n\left(\sqrt{1-{M_0}^2W(0)}\,r\right) \tag{5}$$

Thus an eigenvalue problem for the complex eigenvalue α has to be solved for given values of $U(r)/U_0$, $T(r)/T_0$, M_0, ω and n, which are satisfying the following *dispersion relation*.

$$F(\alpha, n, \omega; M_0)=0 \tag{6}$$

This relation can be calculated explicitly. For more realistic velocity profiles, the result is obtained by numerically integrating Eq. (2) for a chosen value of α, and the value then continues to be changed until the boundary conditions (4) and (5) are satisfied.

2.1. Temporal and spatial theories

When we consider *temporal* instability growth, α becomes real and ω becomes complex: $\omega=\omega_r+i\omega_i$. Equation (1) then takes this form:

$$v' = \tilde{v}(r)e^{\omega_i t}e^{in\phi+i(\alpha x-\omega_r t)} \tag{7}$$

Depending on the sign of the temporal amplification rate ω_i, the disturbances are damped for $\omega_i < 0$, amplified for $\omega_i > 0$, and neutral for $\omega_i = 0$. ω_r represents the frequency and α the wave number in the x direction.

On the other hand, when we consider *spatial* instability growth, ω becomes real and α becomes complex: $\alpha = \alpha_r + i\alpha_i$. As a result, Eq. (1) is expressed by

$$v' = \tilde{v}(r)e^{\alpha_i x}e^{in\phi + i(\alpha_i x - \omega t)} \tag{8}$$

In this case, the fluctuation can be amplified for $\alpha_i < 0$, neutral for $\alpha_i = 0$, and damped for $\alpha_i > 0$ in the x direction.

From these definitions, it is clear that any eigenvalue problem involves three real parameters; that is, they are (α, ω_i, ω_r) for temporal growth, and (α_r, α_i, ω) for spatial growth.

The mean velocity and temperature profiles have to be given as input. The latter can be related to the former by using the Busemann-Crocco law that is valid for a boundary layer flow with a constant pressure and $Pr = 1$.

$$\frac{T(r)}{T_0} = \frac{T_\infty}{T_0} + \left(1 - \frac{T_\infty}{T_0}\right)\frac{U(r)}{U_0} + \frac{(\gamma - 1)M_0{}^2}{2}\frac{U(r)}{U_0}\left(1 - \frac{U(r)}{U_0}\right) \tag{9}$$

Here, T_∞ / T_0 is the ratio of ambient temperature to jet centerline temperature, $U(r)$ is the jet axial velocity, U_0 is the centerline velocity, and γ the ratio of specific heats. Besides these values, other inputs are M_0, T_0, and n. One of the real value parameters mentioned above also has to be given to complete this calculation, which is α for temporal growth and ω for spatial growth. Two remaining parameters will be obtained as eigenvalues as a result of calculation, as well as the disturbance amplitude profiles as eigenfunctions.

In the present analysis the velocity profile was given as the following hyperbolic-tangent form.

$$\frac{U(r)}{U_0} = \frac{1}{2}\left[1 + \tanh\left\{0.25\frac{R}{\theta}\left(\frac{R}{r} - \frac{r}{R}\right)\right\}\right] \tag{10}$$

where θ is the momentum thickness defined as

$$\theta = \int_0^\infty \left(\frac{\rho(r)}{\rho_0}\right)\left(\frac{U(r)}{U_0}\right)\left(1 - \frac{U(r)}{U_0}\right)dr \tag{11}$$

Michalke,[5] Chan and Leong,[6] Morris,[7] Crigthon and Gaster,[8] and Plaschko[9] have employed this profile for their jet stability analyses.

In general, in compressible flows the mean flow density, $\bar{\rho}(r)$, also changes with the location. For an ideal gas, the equation of state can give the following relation between the density and temperature for a constant pressure field.

$$\frac{T(r)}{T_0} = \left[\frac{\rho(r)}{\rho_0}\right]^{-1} \tag{12}$$

2.2. Relation between spatial and temporal instability theories

It is possible to convert a temporal to a spatial amplification rate by using the concept of group velocity that represents the velocity at which energy propagates in a conservative system. In the temporal instability growth theory, the group velocity C_g is defined by[10,11]

$$C_g = \frac{\partial \omega_r}{\partial \alpha} \tag{13}$$

It can be demonstrated that the temporal growth rate, ω_i, can be converted to a spatial growth rate, $-\alpha_i$, by the following relation:

$$-\alpha_i = \frac{\omega_i}{C_g} \tag{14}$$

In principle, the relation (14) is only valid for small values of ω_i, i.e., in the neighborhood of a neutral point.

2.3. Physical disturbances (wave amplitude)

The physical disturbances correspond to the real parts of Eq. (1). When the spatial growth theory is applied to axisymmetric disturbances with $n = 0$, the physical disturbance, $v_{\text{physical}}{}'$, is expressed by

$$v_{\text{physical}}{}' = |v(r)|e^{-\alpha_i x}\cos(\alpha_r x - \omega t + \varphi(r)) \tag{15}$$

where

$$|\tilde{v}| = (\tilde{v}_r{}^2 + \tilde{v}_i{}^2)^{1/2}, \quad \cos\varphi = \tilde{v}_r/|\tilde{v}|, \quad \text{and} \quad \sin\varphi = \tilde{v}_i/|\tilde{v}|$$

$\tilde{v}_{\text{physical}}{}'$ is the root mean square value of $v_{\text{physical}}{}'$, which is obtained by integrating Eq. (15) over one temporal period:

$$\tilde{v}_{\text{physical}}{}' = \frac{1}{\sqrt{2}}|v(r)|e^{-\alpha_i x} \tag{16}$$

If A represents the magnitude of $\tilde{v}_{\text{physical}}{}'$, we have

$$\frac{1}{A}\frac{dA}{dx} = -\alpha_i \tag{17}$$

This equation is valid for any value of radial site r.[2,12]

3. Principle of the e^N Method

The principle of this method is described here for two-dimensional incompressible boundary layer flows. A laminar basic flow is specified, which can be either computed or measured, so that the mean velocity profiles are available at a large number of streamwise locations x_j. Then a local stability analysis for this basic flow is performed at each location of x_j to determine the amplification, or growth rate, for locally unstable disturbances. These calculations enable us to obtain a stability diagram that shows a range of amplified Tollmien-Shlichting waves as a function of streamwise location, which is shown in the upper part of Fig. 1.

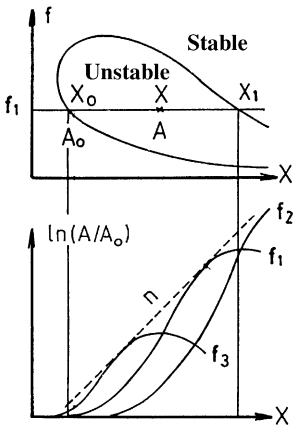

Fig. 1. Principle of the e^N method [D. Arnal[2]].

Here we consider a wave that propagates downstream with a physical frequency f_1. Figure 1 shows that this wave travels first through a stable region; that is, it can be damped up to $x = x_0$. Then it is amplified up to $x = x_1$ and damped after that. At any location with $x > x_0$, the wave amplitude A can be related to the amplitude A_0 at the neutral point x_0 by integrating the Eq. (17). In the framework of the spatial instability growth theory, this is expressed by

$$\frac{A}{A_0} = \exp\left\{\int_{x_0}^{x} -\alpha_i dx\right\} \quad \text{or} \quad \ln\left(\frac{A}{A_0}\right) = \int_{x_0}^{x} -\alpha_i dx \tag{18}$$

where A_0 is usually called the initial disturbance amplitude. This value is linked to the surrounding disturbance environment through some receptivity mechanism. The streamwise variation of the natural logarithm of A/A_0 is plotted in the lower part of Fig. 1 for the frequency f_1 as well as for other frequencies f_2, f_3, etc. It is obvious from Eq. (18) that $\ln(A/A_0) = 0$ at $x = x_0$ and that the slopes of the curves vanish at $x = x_0$ and $x = x_1$. The dashed line in Fig. 1 represents an envelope for these curves, which is called the factor of N.[2)]

$$N = \max_f \left[\ln\left(\frac{A}{A_0}\right)\right] \tag{19}$$

At each streamwise location of x, N represents the maximum amplification factor of the disturbances.[2)]

So far, the only assumption is the use of the linear stability theory. Unfortunately, it is not sufficient to determine the transition location. Therefore if it is predicted with this method, an additional assumption is needed, which was suggested independently by Smith and Gamberoni[3)] and by Van Ingen.[4)] They collected many experimental transition data and found that the N factor attains nearly a constant value between 7 and 9 at the measured transition point. This means that a transition occurs when the amplitude of most amplified Tollmien-Schlichting waves attains the value from e^7 (= 1,097) to e^9 (= 8,103) times as large as its initial amplitude, A_0.

Here we summarize the procedure needed when this method, which consists of three steps, is applied:

1. Accurate calculation or measurement for the laminar velocity profile at each station.
2. Stability calculations for these profiles.
3. Integration of the local growth rate to define an envelope curve. The transition location is then easily determined if a threshold value of the N factor is specified.

Nonlinear mechanisms and receptivity are not considered in this method. Therefore they are shortcomings in the e^N method.[2)] However, the e^N method is certainly the most popular technique used today as a practical transition prediction tool.

The main objective of the present study is to correlate stability calculations with the transition location of a compressible jet's free shear layer in the same way as the e^N method regarding boundary layer, and to determine the value of N in the present jet flow.

4. Results and Discussion

4.1. Mean flow field of compressible jet

In the present study, the mean flow field was determined experimentally. All measurements were conducted in the open jet facility at the Fluid Dynamics Laboratory, Department of Aerospace Engineering, Nagoya University. A detailed description of the facility can be found in Ref. 13. The flow of jet is issued from a convergent nozzle having an exit diameter, D, of 7.5 mm. M_j is commonly used to denote the fully expanded Mach number, which is one of the jet's characteristics. It has a unique relation with the nozzle pressure ratio, *NPR,* which is defined by P_t/p_∞ by the following equation:

$$M_j = \left\{\left[\left(\frac{P_t}{p_\infty}\right)^{\gamma-1/\gamma} - 1\right]\frac{2}{\gamma-1}\right\}^{0.5} \tag{20}$$

The jet considered in the present study is a sonic jet, i.e., $M_j = 1.00$, which corresponds to $NPR = 1.89$. The corresponding Reynolds number is $Re = 1.5\times10^5$, which is based on the nozzle exit diameter and the primary jet velocity.

Figure 2 shows a distribution of the centerline Mach number, which was obtained only by pitot probe measurements. Therefore the Mach number was calculated by using the isentropic flow relation of Eq. (20), where P_t in this case represents the local pitot pressure.

The potential core length is defined as the distance measured in the axial direction from the nozzle exit to where the inner edge of the ring-shaped jet shear layer merges to a point at the axis. This length can be determined easily in a fully expanded jet, where the centerline Mach number remains constant until this merging point, and decreases monotonically downstream of it. Here in this study, the downstream end of the potential core was defined as the location where the centerline Mach number drops to a certain level, specifically 5%, below the nozzle exit Mach number. Thus we have a potential core length of about $5D$ for the present jet. The vertical lines shown in Fig. 2 represent the axial locations at which the axial velocity component was measured along each radial coordinate.

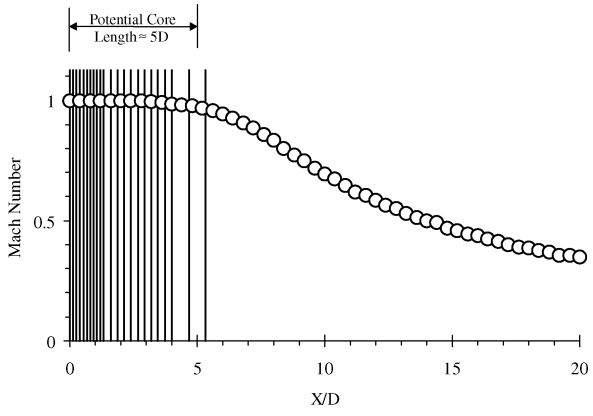

Fig. 2. Centerline Mach number distribution.

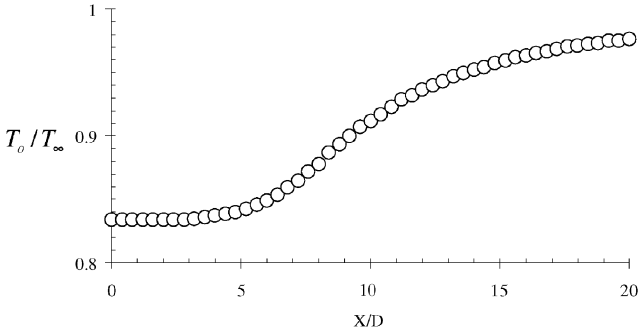

Fig. 3. Jet centerline temperature distribution normalized by ambient temperature.

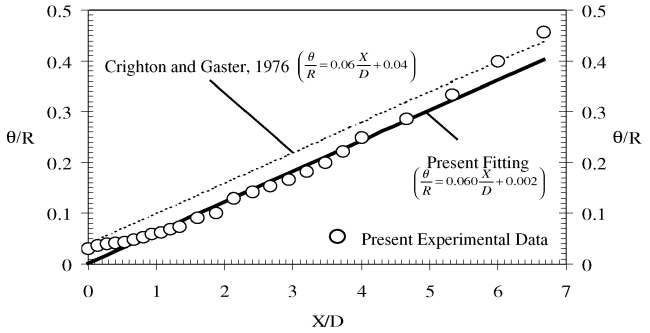

Fig. 5. Axial variation of the ratio of momentum thickness to jet radius, θ/R.

Figure 3 shows the centerline distribution of T_0/T_∞ ratio. This ratio was calculated from the centerline Mach number distribution by the use of an isentropic relation. This parameter is indispensable for calculating the temperature profile in stability analysis based on Busemann-Crocco's law of Eq. (9).

The normalized radial Mach number distributions at 25 axial locations from the nozzle exit up to $X/D = 6.667$ are shown in Fig. 4. Besides the experimental data obtained in this study, the least square fitted hyperbolic-tangent velocity profile of Eq. (10) is presented in this figure. In this fitting method, for a given hyperbolic tangent velocity profile, $M_{\text{approx.}}(r_k/R,\, R/\theta)$, and experimental data, $M_{\text{Exp.}}(r_k/R)$,

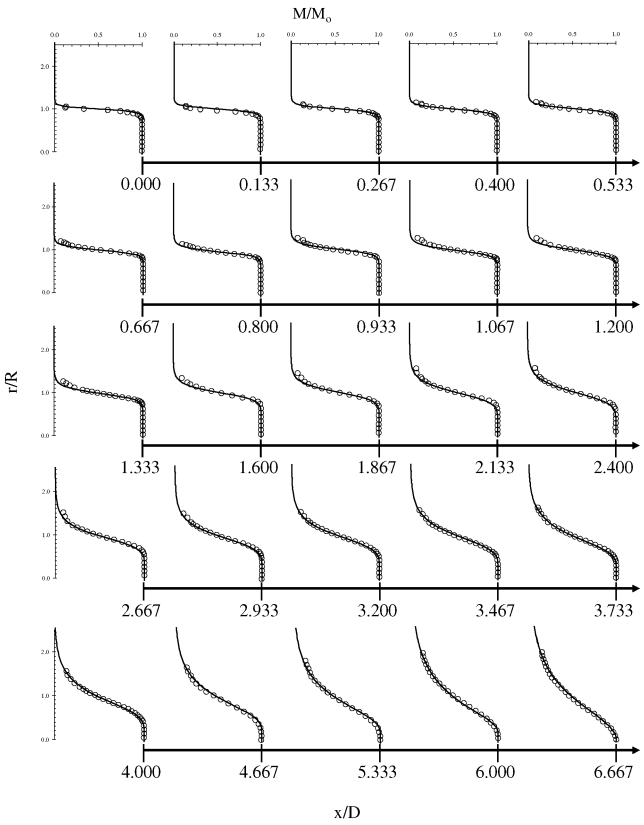

Fig. 4. Radial Mach number distributions at different axial locations. ○: experimental data; —: hyperbolic - tangent velocity profile.

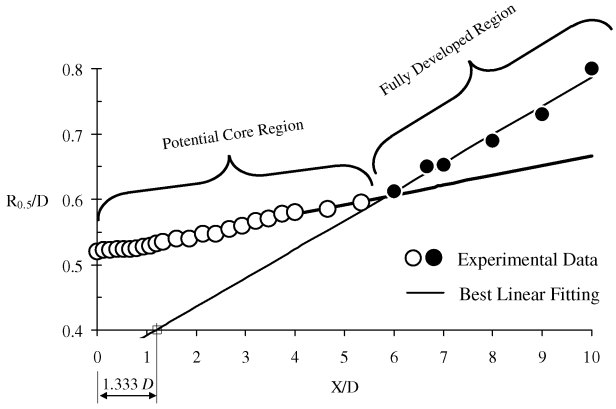

Fig. 6. Axial variation of jet radius R.

where M is Mach number, the optimal value of R/θ is defined by the minimum value of the following term:

$$\sum_{k=1}^{m}\left[M_{\text{Exp.}}(r_k/R) - M_{\text{approx}}(r_k/R,\, R/\theta)\right]^2 \qquad (21)$$

where m is the number of experimental data points.

As a result of this fitting, we can calculate the variation of θ/R in the axial direction, the result of which is shown in Fig. 5 as well as the data by Crigthon and Gaster[8] for comparison. The fitted straight line has the same slope as that of Crigthon and Gaster,[8] but a different value of the constant. This constant seems to depend on jet initial conditions at the nozzle exit. Note that the value of R/θ at each location is needed to decide the hyperbolic-tangent velocity profile presented in Fig. 4.

Figure 6 shows the axial distribution of jet radius defined as the length from the axis to where the velocity becomes half the centerline velocity at each station.[14] There are two distinct axial regions seen in the figure; one is a potential core region, and the other is a fully developed jet region. The best linear fitting lines as well as these experimental data are presented in the figure. The fully developed region seems to grow from an "apparent origin" at about $X/D = 1.333$.

4.2. Jet linear stability calculations

Inviscid spatial stability analysis has been performed for the present jet flow. The jet linear stability code employed

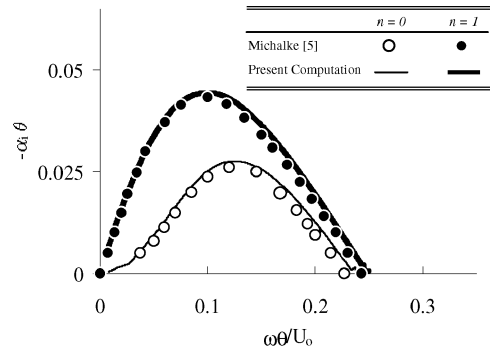

Fig. 7. Jet linear stability test case of the hyperbolic-tangent velocity profile (Eq. 10) with $R/\theta = 6.25$, $M_0 = 1.2$ and $T_0/T_\infty = 1$ (isothermal flow).

here was first validated by comparing it with previously published computations by Michalke[5] for the hyperbolic-tangent velocity profile of Eq. (10) with $R/\theta = 6.25$, $M_0 = 1.2$ and $T_0/T_\infty = 1$, which is an isothermal flow, the results of which are shown in Fig. 7. This figure presents axial growth rate, $-\alpha_i$, normalized by the momentum thickness, versus radian frequency, ω, normalized by the momentum thickness and centerline jet velocity. The present computations have a reasonable agreement with Michalke's results for both axisymmetric ($n = 0$) and asymmetric ($n = 1$) disturbance modes.

The results of stability calculation based on the velocity profiles presented in Fig. 4 are shown in Fig. 8 for axisymmetric disturbances with $n = 0$. The quantities are nondimensionalized by the local momentum thickness and local centerline jet velocity, and the corresponding dimensional results are shown in Fig. 9. We can clearly see a neutral stability curve in this figure, where in the downstream a single neutral frequency exists at each axial location.

The thin axisymmetric shear layer is unstable for a large number discrete azimuthal modes,[9] but a fully developed jet is unstable to the first azimuthal mode, i.e., $n = 1$, at some distance beyond the termination of the potential core.[15] Cohen and Wygnanski[16] showed that as R/θ decreases, the importance of higher azimuthal modes ($n \geq 2$) relatively diminishes, and only the first azimuthal ($n = 1$) and the axisymmetric ($n = 0$) modes remain amplified at the end of the potential core. Therefore in the present study, only these two modes will be considered, whose calculated growth rates are illustrated in Fig. 10 for six axial locations. As we go down-

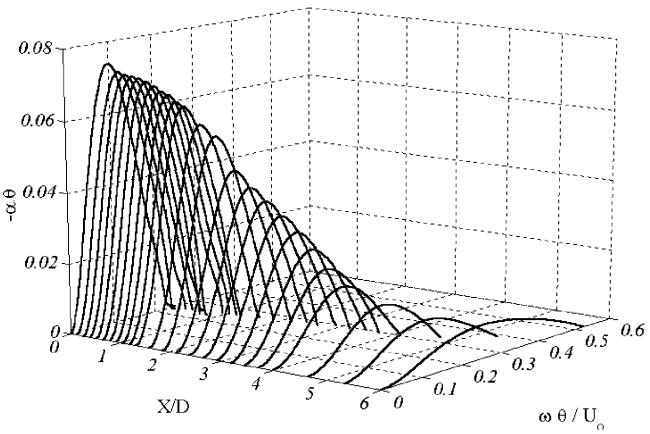

a. Stability curves at different axial locations.

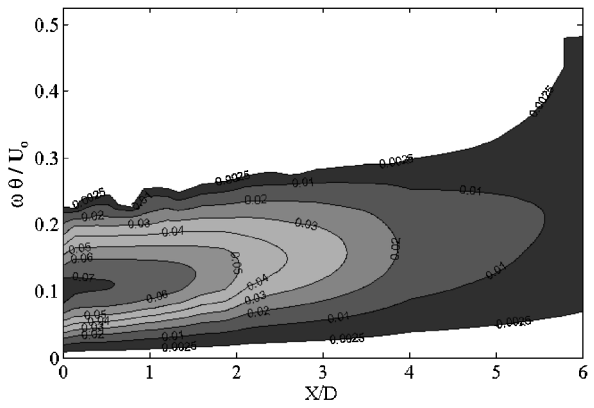

b. Growth rate contours.

Fig. 8. Nondimensional stability curves at different axial locations for the axisymmetric disturbance mode ($n = 0$).

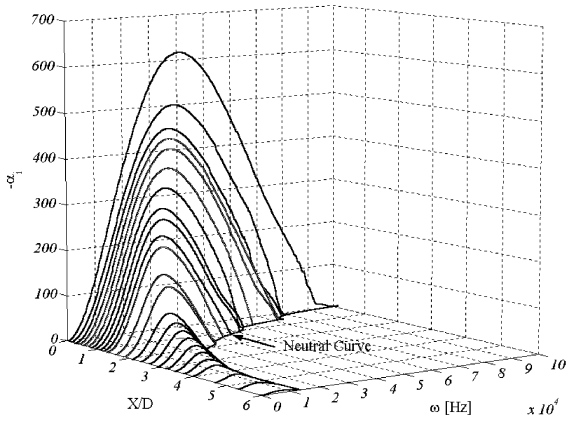

a. Stability curves at different axial locations.

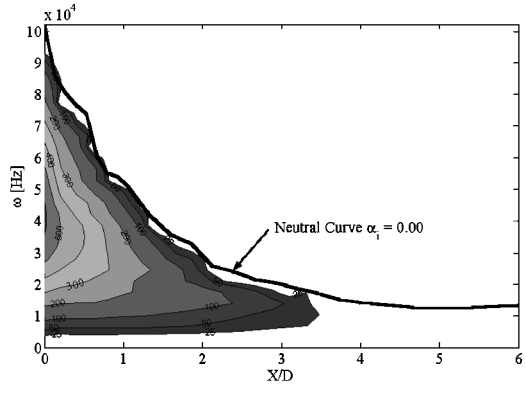

b. Growth rate contours and neutral stability curve.

Fig. 9. Dimensional stability curves at different axial locations for the axisymmetric disturbance mode ($n = 0$).

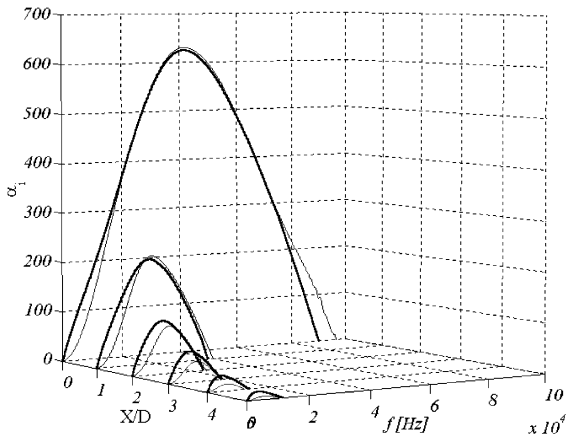

Fig. 10. Dimensional stability curves at different axial locations for " —— " axisymmetric ($n = 0$); " —— " asymmetric ($n = 1$) disturbance modes.

stream, it turns out that the antisymmetric disturbances become more unstable than the axisymmetric ones.

4.3. Transition detection

Transition starts when turbulent structures or spots first appear in the laminar shear layer. Under natural conditions, the spots originate in a more or less random fashion. Once created, they are swept along in the mean flow, growing axially and laterally, and finally cover the entire surface. The transition region is defined as where the turbulent spots grow, overlap, and begin to form a turbulent shear layer. When a hot wire is placed in this region, both the turbulent spots and laminar flow will successively appear in the recorded fluctuation data. This is referred to as the intermittency phenomenon.[2] In this study, three methods are employed to detect the transition location of the jet shear layer flow under consideration, which will be described in the following.

4.3.1. Oil flow visualization

Any visualization technique using Schlieren photography cannot be employed for the transition detection of the jet flow under consideration, because the density variations are too low to detect a change in flow behavior inside the jet plume. The smoke visualization cannot be used either, because the main flow velocity is too high to observe. To overcome these difficulties, we attempted oil flow visualization. We placed a thin plate painted with oil and with a thickness of 0.5 mm, in a meridian plane of the jet, as shown in Fig. 11a, and a video camera captured the time evolution of the oil flow on the surface during the experiment.

Although the plate is very thin compared with the nozzle exit diameter, the effect of its intrusion inside the jet plume on the transition location will exist. The results of the oil flow visualization are shown in Fig. 11b. Turbulent spots can be clearly recognized as white spots near the jet boundary, whose origin lies between $1D$ and $2D$. As mentioned earlier, the present oil flow results might have some differences from a real jet flow. One important issue in this visualization is to determine the jet boundary. Since the accuracy of the pressure transducers is poor in low-speed regions, it is

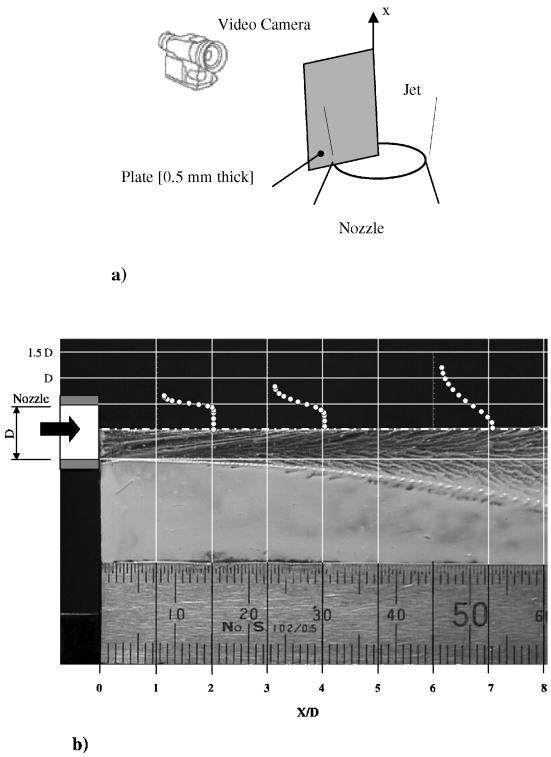

Fig. 11. Oil flow visualization: a) Experimental arrangement for oil flow visualization; b) Jet boundary visualized by oil flow.

difficult to determine the jet boundary only by pitot pressure measurements. The determination of the jet boundary will be very helpful in specifying the transition location by using a microphone or a hot-wire anemometer, which will be discussed next.

4.3.2. Pressure fluctuations measured by microphone

One method to detect the transition location is the use of a microphone to measure the pressure fluctuations of a jet flow. In the present method, the microphone was moved along a line parallel to the jet boundary determined by the oil flow visualization mentioned above. Specifically, the line was away from the jet boundary by $0.8D$, as shown

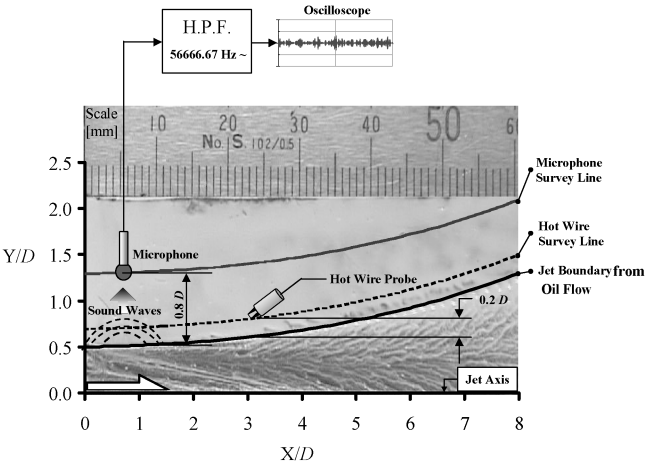

Fig. 12. Experimental setup for transition detection.

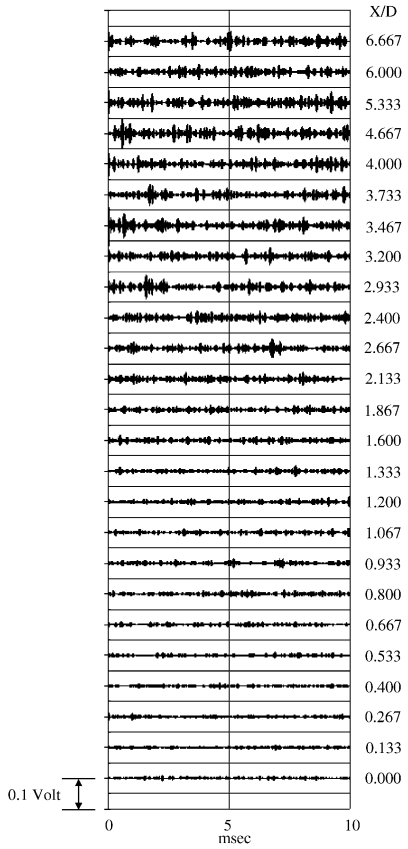

Fig. 13. HPF microphone signals at different axial locations.

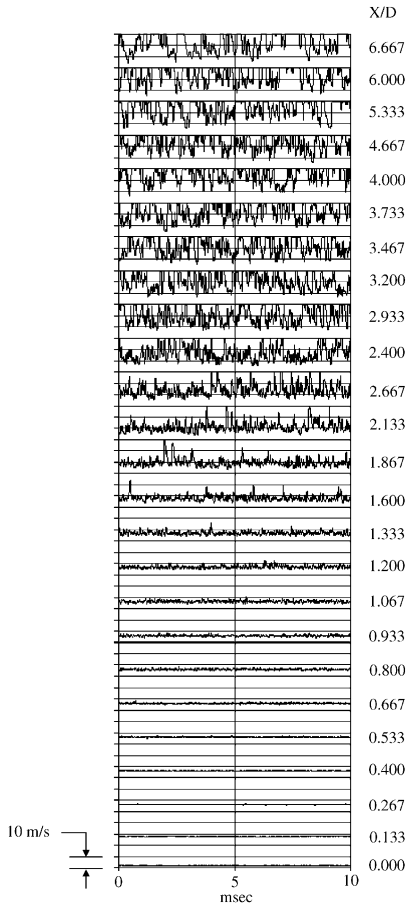

Fig. 14. Velocity fluctuations measured by hot wire at different axial locations.

in Fig. 12. The microphone at this location can catch only sound waves with wavelengths of less than $0.8D$ produced by the jet shear layer. This means that the microphone signal has to be high-pass-filtered, the lowest frequency of which has a wavelength of $0.8D$. The resulting signals are shown in Fig. 13 at different downstream locations from the nozzle exit. In this figure, regular peak patterns start to appear from approximately $x \approx 1.6D$, whose location is considered to be the onset of the turbulent spots, or transition.

4.3.3. Velocity fluctuations measured by hot wire

Transition detection by the use of a hot-wire anemometer is one of the well-documented methods of measuring velocity fluctuations.[2)] In the present experiment, a hot-wire was traversed along a line parallel to the jet boundary, which was away from it by $0.2D$ to avoid hot-wire damage because of the high-speed jet flow. The velocity fluctuations measured by the hot-wire at various downstream locations are shown in Fig. 14. We can clearly see that the turbulent spots begin to appear at approximately $x = 1.333D$. This is not so different from $1.6D$ by the microphone mentioned above and seems to be also in reasonable agreement with the transition location between $x = 1D$ and $2D$ because of the oil flow visualization. It is very interesting to notice that the transition location determined by the hot-wire anemometer is very close to the "apparent origin" of the fully developed jet flow, as shown in Fig. 6.

4.4. Envelope curve

The spatial growth rate, $-\alpha_i$, has been integrated based on Eq. (18) to obtain an envelope curve similar to that of a boundary layer flow presented in Fig. 1. The lower limit of the integration is the nozzle exit, i.e., $x = 0$. The results of spatial growth rate integration for a selected set of frequencies for axisymmetric disturbance modes ($n = 0$) are shown in Fig. 15a. These integration curves represent the streamwise variations of the natural logarithm of A/A_0, and the thick solid line is the envelope of these curves, which is called the factor of N.[2)]

Based on both microphone and hot-wire measurements, the transition location seems to be between $x = 1.333D$ and $x = 1.6D$. The microphone has a diameter of about 0.125 inch, which might affect its resolution regarding the transition location. Therefore hot-wire measurements seem to be more accurate than the microphone in terms of the transition location. Thus, $x = 1.333D$ is considered to be the onset of the transition region in this study. The corresponding N factor is about 3.5 for axisymmetric disturbance modes ($n = 0$), as shown in Fig. 15a. Figure 15b shows the same results for the first azimuthal disturbance modes ($n = 1$). In this case, the factor N, which corresponds to $x = 1.333D$, becomes about 2.8. That is, this

difference in the value of N suggests that the axisymmetric disturbances can be more amplified in this region than the asymmetric ones can. This is consistent with the results of Cohen and Wygnanski,[16] who showed that first azimuthal disturbance modes are more amplified than the axisymmetric disturbance modes near the end of the potential core only. Therefore transition prediction based on the stability computations of axisymmetric disturbance modes should be more accurate than the asymmetric ones. The natural logarithm of A/A_0 for the first azimuthal disturbance modes with low frequencies is higher in magnitude than that of the axisymmetric disturbance modes. This is confirmed because the antisymmetric ($n = 1$) disturbances are more unstable than the axisymmetric at low frequencies, as presented earlier in Fig. 10.

For boundary layer flow, the transition location was correlated with the N factor from 7 to 9. This variation in the N factor was found to be due to a variation in the free-stream turbulence level.[12] An increase in this level will decrease the transition Reynolds number, and consequently the N factor will have a low value and vice versa.

No attempt has been made for the present study to investigate the effect of the jet upstream turbulence level on N factor and the transition location. From the value of N factor based on stability computation of the axisymmetric disturbance modes, a transition is believed to occur when the amplitude of the most amplified waves becomes $e^{3.5}$ (= 33) times as large as its initial amplitude, A_0. On the other hand, in a boundary layer flow, where the low limit of N factor is 7, the transition occurs when the amplitude of the most amplified waves becomes e^7 (= 1,097) times as large as its initial amplitude, A_0. A comparison of these values of N factor asserts that the boundary layer flow is more stable than the free shear flow.

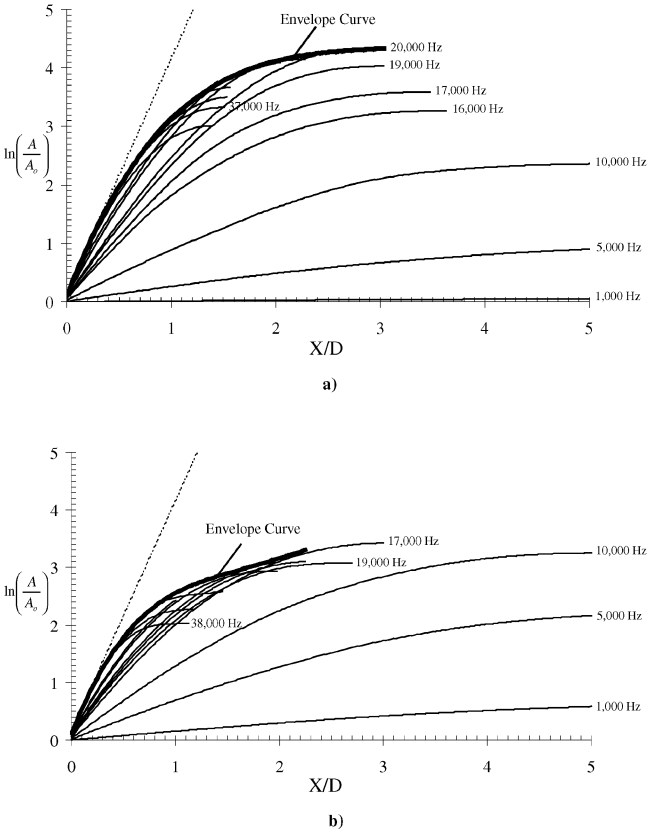

Fig. 15. Envelope curve for instability growth: a) Axisymmetric disturbance modes ($n = 0$); b) Asymmetric disturbance mode ($n = 1$).

5. Conclusion

A correlation between the linear stability calculations of a compressible jet flow and the onset of its transition location has been established. The spatial stability theory is considered in the present study. The jet mean velocity profiles were obtained experimentally at different downstream locations. The stability calculations were performed for these profiles and integrated to obtain an envelope curve. The transition was observed experimentally by using an oil flow visualization, a microphone for pressure fluctuation, and a hot-wire anemometer for velocity fluctuation. Results from both the microphone and hot-wire measurements determined the transition location to be about $x = 1.333D$, where D is the nozzle diameter. This is very close to the location of the "apparent origin" in the fully developed jet flow. It was found that the value of N factor is about 3.5 for the axisymmetric disturbance mode ($n = 0$) and 2.8 for the asymmetric ($n = 1$) disturbance mode. This difference in the value of N suggests that the axisymmetric disturbance mode can be more amplified in this upstream region than the asymmetric one. Therefore a prediction based on the stability computations of axisymmetric disturbance mode should be more accurate than that based on asymmetric one. Further work is still required to investigate the effect of the jet upstream turbulence level on the value of N factor as well as the transition location.

References

1) Morkovin, M. V.: Critical Evaluation of Transition from Laminar to Turbulent Shear Layers with Emphasis on Hypersonically Travelling Bodies, Report AFFDL-TR-68-149, Wright-Patterson Air Force Base, Ohio, 1968.
2) Arnal, D.: Prediction Based on Linear Theory, In Progress in Transition Modeling, AGARD Report No. 793, 1993, pp. 2/1–2/63.
3) Smith, A. M. O. and Gamberoni, N.: Transition, Pressure Gradient and Stability Theory, Douglas Aircraft Co., Report ES 26388, El Segundo, California, 1956.
4) Van Ingen, J. L.: A Suggested Semi-Empirical Method for the Calculation of the Boundary Layer Transition Region, University of Techn., Dept. of Aerospace Eng., Report UTH-74, Delft, 1956.
5) Michalke, A.: Survay on Jet Instability Theory, *Prog. Aerospace Sci.*, **21** (1984), pp. 159–199.
6) Chan, Y. Y. and Leong, R. K.: Discrete Acoustic Radiation Generated by Jet Instability, *Can. Aeronaut. Space Inst. Trans.*, **6** (1973), pp. 65–72.
7) Morris, P. J.: The Spatial Viscous Instability of Axisymmetric Jets, *J. Fluid Mech.*, **77** (1976), pp. 511–529.
8) Crighton, D. G. and Gaster, M.: Stability of Slowly Diverging Jet Flow, *J. Fluid Mech.*, **77** (1976), pp. 397–413.
9) Plaschko, P.: Helical Instabilities of Slowly Diverging Jets, *J. Fluid Mech.*, **92** (1979), pp. 209–215.

10) Schlichting, H.: *Zur Entstehug der Turbulenz bei der Plattenströmunggesellschaft der Wissenschaften*, Math-Phys., Klasse, Göttingen, 1933, pp. 181–208.
11) Gaster, M. A.: A Note on the Relation between Temporally Increasing and Spatially Increasing Disturbances in Hydrodynamic Stability, *J. Fluid Mech.*, **14** (1962), pp. 222–224.
12) Mack, L. M.: Transition Prediction and Linear Stability Theory, AGARD Conf. Proc., No. 224, Paris, 1977.
13) Ibrahim, M. K. and Nakamura, Y.: Flow Field and Noise Characteristics Due to Supersonic Jet Shear-Layer Vortex Interaction, AIAA Paper 2000–2533, 2000.
14) Troutt, T. R. and Mclaughin, D. K.: Experiments on the Flow and Acoustic Properties of a Moderate-Reynolds-Number Supersonic Jet, *J. Fluid Mech.*, **116** (1982), pp. 123–156.
15) Batchelor, G. K. and Gill, A.: Analysis of the Stability of Axisymmetric Jets, *J. Fluid Mech.*, **14** (1962), pp. 529–551.
16) Cohen, J. and Wygnanski, I.: Evolution of Instabilities in the Axisymmetric Jet. Part 1: The Linear Growth of Disturbance Near the Nozzle, *J. Fluid Mech.*, **176** (1982), pp. 191–219.